Inorganica Chimica Acta 514 (2021) 119972

Contents lists available at ScienceDirect

Inorganica Chimica Acta

journal homepage: www.elsevier.com/locate/ica

Research paper

The influence of α,α′-diimine bridging ligand on the reactivity of binuclear *para*-cymene ruthenium(II) complexes. Kinetic, mechanistic and computational study

Gershom Kyalo Mutua[a,b,*], Daniel O. Onunga[a], Meshack Sitati[a], Deogratius Jaganyi[c,d,*], Allen Mambanda[a]

[a] School of Chemistry and Physics, University of KwaZulu-Natal, Private Bag X01, Scottsville, Pietermaritzburg, 3209, South Africa
[b] Department of Pure and Applied Chemistry, School of Natural Sciences, Masinde Muliro University of Science and Technology, P.O Box 190, Kakamega 50100, Kenya
[c] School of Pure and Applied Sciences, Mount Kenya University, P.O. Box 342-01000, Thika, Kenya
[d] Department of Chemistry, Faculty of Applied Sciences, Durban University of Technology, P.O Box 1334, Durban 4000, South Africa

ARTICLE INFO

Keywords:
Binuclear ruthenium(II)
Substitution
Kinetics
Thiourea
Bridging ligand

ABSTRACT

Substitution kinetics of the aqua ligands in four binuclear ruthenium(II) *para*-cymene complexes with different α,α′-diimine bridging ligands [2-pyridylaldazine (Ru-1), *p*-phenylene*bis*(picoline)aldimine (Ru-2), *p*-biphenylene*bis*(picoline)aldimine (Ru-3) and *p*-xylene*bis*(picoline)aldimine (Ru-4)] was investigated as a function of nucleophile concentration and temperature under *pseudo*-first order conditions using thiourea nucleophiles. The rates of the simultaneous substitution of the aqua ligands decreased in the order: Ru-1 > Ru-4 > Ru-3 > Ru-2. The reactivity of the complexes is controlled by the inherent electronic and steric contributions of the bridging ligand. The strong π-acceptor bridging ligand is responsible for the high reactivity observed in Ru-1 compared to the rest of the complexes. From Ru-2 to Ru-4, the reactivity increases with decrease in steric congestion around the metal centres. The cage effect plays a role in the enhanced reactivity of Ru-4 compared to Ru-3 and Ru-2. Reactivity trends are excellently supported by computational results. All the complexes showed a stepwise deprotonation of the coordinated aqua ligands except Ru-4 and the p*K*a values increased from Ru-1 to Ru-4 due to progressive increase in σ-donicity of the spacers. The activation parameters ($\Delta H^{\neq} > 0$, $\Delta S^{\neq} < 0$) obtained for all the complexes support an associative mechanism of activation.

1. Introduction

Pseudo-octahedral half-sandwich ruthenium(II) complexes forms an important class of ruthenium complexes with vast applications in areas such as catalysis and anti-cancer drug design [1–3]. These complexes are amphiphilic in nature because of their hydrophobic arene moiety and the hydrophilic metal centre. The π-bonded arene ligand occupy three coordination sites and the remaining three sites offer diverse coordination modes that can be utilized for tailored complexes [3]. Multinuclearity is an emerging approach in the design of metal complexes for application in different areas. This is because multinuclear complexes are more active than their mononuclear analogues because of synergistic effects [4,5]. The bridging ligand modulates the properties of these complexes as well as provide steric protection to the metal centres against non-target molecules [6,7].

Extensive studies investigating the effect of the bridging ligand on substitution kinetics of square-planar platinum(II) complexes have been reported [8–12]. It is established that the effect of the linker on reactivity is entirely dependent on the intrinsic properties therein. These include; the net σ-inductive effect of the linker, magnitude of the steric hindrance introduced by the linker, the rigidity/flexibility of the linker [8,9], the length of the linker [10–12], the head group that coordinates the metal centres and the symmetry of the complexes [9,13]. Due to synergistic or antagonistic factors, the role of a bridging ligand on the reactivity of transition metal complexes is specific to the chemistry of the complex and the bridging ligand. In addition, there is limited literature about the structure–reactivity relationship on binuclear ruthenium(II) arene complexes [14].

The current work was undertaken to understand the role of non-aliphatic bridging ligands on the reactivity of ruthenium(II) *para*-

* Corresponding authors at: School of Chemistry and Physics, University of KwaZulu-Natal, Private Bag X01, Scottsville, Pietermaritzburg, 3209, South Africa (G. Kyalo Mutua). School of Pure and Applied Sciences, Mount Kenya University, P.O. Box 342-01000, Thika, Kenya (D. Jaganyi).
E-mail addresses: gkmutua@rocketmail.com (G.K. Mutua), deojaganyi@gmail.com (D. Jaganyi).

https://doi.org/10.1016/j.ica.2020.119972
Received 20 February 2020; Received in revised form 10 August 2020; Accepted 23 August 2020
Available online 26 August 2020
0020-1693/

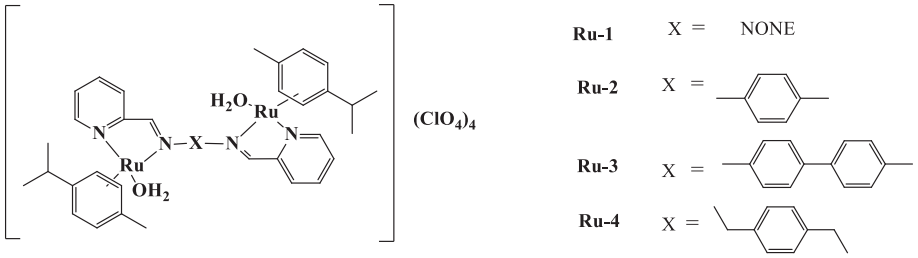

Fig. 1. Structures of the investigated ruthenium(II) complexes.

cymene complexes. To achieve this, four already reported complexes with α,α′-diimine bridging ligands; *viz*. 2-pyridylaldazine (Ru-1), *p*-phenylene*bis*(picoline)aldimine (Ru-2), *p*-biphenylene*bis*(picoline)aldimine (Ru-3) and *p*-xylene*bis*(picoline)aldimine (Ru-4) (Fig. 1) were studied.

Because of their biological importance, high solubility and nucleophilicity, neutral thiourea nucleophiles of varying steric demands were used [15]. These are; thiourea (Tu), 1,3-dimethylthiourea (Dmtu) and *1,1,3,3*-tetramethylthiourea (Tmtu). Computational studies were performed to assist in understanding and interpreting the experimental results obtained.

2. Experimental

2.1. Materials and procedures

All the syntheses were performed under dinitrogen atmosphere using standard Schlenk techniques. Benzidine (≥98%), 2-pyridinecarbaldehyde (99%), hydrazine hydrate solution (80% in H_2O), *p*-phenylenediamine (≥99%), *p*-xylenediamine (99%), dichlorido(*p*-cymene)ruthenium(II) dimer (97%), $NaBF_4$ (98%), anhydrous $AgClO_4$ (97%), $NaClO_4{\cdot}H_2O$ (98%), $HClO_4$ (70 wt% solution), celite (® 545), pH standard reference solutions (4.0, 7.0 and 10.0), Tu (≥99%), Dmtu (99%) and Tmtu (98%) were supplied by Sigma-Aldrich. Organic solvents were purchased from Merck (Pty) and used without further purification. Ultrapure deionized water from Modulab system was used in the relevant reactions. The ligands and complexes were synthesized according to published literature methods [16–18].

2.2. Physical measurements and instrumentation

Bruker Avance DPX III 400/500 MHz spectrometer fitted with 5 mm probe was used to record ^1H and ^{13}C NMR spectra of the ligands and complexes. All the chemical shifts were expressed in parts per million (ppm) and referenced to trimethylsilane. Electrospray ionization (ESI^+) mass spectra were recorded on a Time of Flight (TOF) Micromass spectrometer. NMR and MS spectra obtained are presented in the Supplementary Information (Figures SI 13–36). Elemental analyses of C, H, and N of the samples were done using Thermo Scientific Flash 2000 analyzer. Agilent technologies Cary 100 Series ultraviolet–visible spectrophotometer equipped with a temperature control unit (accuracy of ± 0.05 °C) was used for p*K*a titrations and kinetic studies. Jenway 4330 combined pH and conductivity meter with a 4.5 mm diameter microelectrode was used to determine the pH of the aqueous complex solutions during p*K*a titrations and before kinetic studies. Before use, the electrode was calibrated with pH 4.0, 7.0 and 10.0 reference solutions. OriginPro 9.1® program was used to analyze the acid-base titration data and the kinetic data obtained [19].

2.3. Synthesis of ligands

2-pyridylaldazine: 30 mL of ethanolic solution containing 0.99 mL of hydrazine hydrate solution was added drop-wise to 3.55 mL of 2-pyridinecarbaldehyde in 10 mL of ethanol at room temperature under inert dinitrogen environment. As the exothermic reaction ensued, fine yellow needle-like crystalline solids appeared. After 1 h, the product was filtered off and recrystallized from ethanol. Yield: 2.86 g (84%). *Anal. Calc*. for $C_{12}H_{10}N_4$; C, 68.56; H, 4.79; N, 26.65. *Found*: C, 68.52; H, 4.89; N, 26.44. ^1H NMR (400 MHz, benzene-d_6): δ (ppm) = 9.11 (s, 2H, N = CH), 8.55 (d, 2H, $CH_{pyridyl}$), 8.21 (d, 2H, $CH_{pyridyl}$), 7.10 (t, 2H, $CH_{pyridyl}$), 6.69 (t, 2H, $CH_{pyridyl}$). ^{13}C (400 MHz, benzene-d_6): δ (ppm) = 162.5 (N=C), 153.7 ($C_{pyridyl}$), 149.7 ($C_{pyridyl}$), 135.7 ($C_{pyridyl}$), 124.5 ($C_{pyridyl}$), 121.4 ($C_{pyridyl}$). ESI-MS (TOF) (*m/z*): 233.08 (M + Na).

p-phenylene*bis*(picoline)aldimine: 2-pyridinecarbaldehyde (1.32 mL) was added dropwise to a stirring ethanolic solution of *p*-phenylenediamine (0.85 g) maintained at 60 °C. The mixture was refluxed for 2 h and the resulting red solution cooled to 0 °C. The yellow precipitate which formed was filtered off and recrystallized from ethanol. Yield: 2.02 g (90%). *Anal. Calc*. for $C_{18}H_{14}N_4$; C, 75.50; H, 4.93; N, 19.57. *Found*: C, 75.40; H, 5.07; N, 19.34. ^1H NMR (400 MHz, DMSO-d_6): δ (ppm) = 8.75 (d, 2H, $CH_{pyridyl}$), 8.68 (s, 2H, N = CH), 8.19 (d, 2H, $CH_{pyridyl}$), 7.97 (t, 2H, $CH_{pyridyl}$), 7.54 (t, 2H, $CH_{pyridyl}$), 7.47 (s, 4H, CH_{phenyl}). ^{13}C (400 MHz, DMSO-d_6): δ (ppm) = 160.4 ($C_{pyridyl}$), 154.1 (N=C), 149.7 ($C_{pyridyl}$), 149.0 ($C_{pyridyl}$), 137.1 ($C_{pyridyl}$), 125.6 ($C_{pyridyl}$), 122.3 (C_{phenyl}), 121.3 (C_{phenyl}). ESI-MS (TOF) (*m/z*): 309.11 (M + Na).

p-biphenylene*bis*(picoline)aldimine: 2-pyridinecarbaldehyde (0.66 mL) was added drop by drop to a stirring ethanolic solution of benzidine (0.72 g) maintained at 60 °C. The mixture was refluxed for 2 h and the resulting solution cooled to ambient temperature. The yellow crystalline solid formed was filtered off and recrystallized from ethanol. Yield: 1.18 mg (83%). *Anal. Calc*. for $C_{24}H_{18}N_4$; C, 79.54; H, 5.01; N, 15.46. *Found*: C, 79.48; H, 5.12; N, 15.31. ^1H NMR (400 MHz, benzene-d_6): δ (ppm) = 8.98 (s, 2H, N = CH), 8.63 (d, 2H, $CH_{pyridyl}$), 8.43 (d, 2H, $CH_{pyridyl}$), 7.52 (t, 4H, CH_{phenyl}), 7.37 (d, 4H, CH_{phenyl}), 7.20 (t, 2H, $CH_{pyridyl}$), 6.76 (t, 2H, $CH_{pyridyl}$). ^{13}C (400 MHz, benzene-d_6): δ (ppm) = 160.8 (N=C), 155.5 ($C_{pyridyl}$), 150.5 ($C_{pyridyl}$), 149.6 ($C_{pyridyl}$), 139.1 (C_{phenyl}), 135.9 ($C_{pyridyl}$), 124.6 (C_{phenyl}), 121.9 (C_{phenyl}), 121.2 ($C_{pyridyl}$). ESI-MS (TOF) (*m/z*): 385.14 (M + Na).

p-xylene*bis*(picoline)aldimine: 2-pyridinecarbaldehyde (1.06 mL) was added drop by drop to a stirring ethanolic solution of *p*-xylenediamine (0.86 g) maintained at 65 °C. The mixture was refluxed for 3 h and the resulting solution cooled to 0 °C. The off-white precipitate formed was filtered off and recrystallized from ethanol. Yield: 1.62 g (82%). *Anal. Calc*. for $C_{20}H_{18}N_4$; C, 76.41; H, 5.77; N, 17.82. *Found*: C, 76.39; H, 5.51; N, 17.65. ^1H NMR (400 MHz, chloroform-*d*): δ (ppm) = 8.67(d, 2H, $CH_{pyridyl}$), 8.51 (s, 2H, N = CH), 8.08 (d, 2H, $CH_{pyridyl}$), 7.74 (t, 2H, $CH_{pyridyl}$), 7.34 (m, 6H, $CH_{pyridyl}$, CH_{phenyl}), 4.90 (d, 4H, CH_2). ^{13}C (400 MHz, Toluene-d_8) δ (ppm) = 162.7 ($C_{pyridyl}$), 155.4 (N=C), 149.1 ($C_{pyridyl}$), 138.0 ($C_{pyridyl}$), 135.5 (C_{phenyl}), 124.0 (C_{phenyl}), 120.6 ($C_{pyridyl}$), 64.4 (CH_2). ESI-MS (TOF) (*m/z*): 337.14 (M + Na).

2.4. Synthesis of the complexes

A suspension of 1.50 mmol of dichlorido(*p*-cymene)ruthenium(II) dimer in 30 mL of methanol was treated with 1.50 mmol of the ligand (2-pyridylaldazine, *p*-phenylenebis(picoline)aldimine, *p*-biphenylenebis (picoline)aldimine and *p*-xylene-bis(picoline)aldimine) and allowed to

stir at room temperature for 4 h. In each case, solution was filtered through celite to remove unreacted materials. 3.10 mmol of $NaBF_4$ in 10 mL of methanol was then added to the filtrate. The resulting solution was kept in the refrigerator for slow crystallization to take place. After a few days, the crystalline tetraflouroborate salts which formed were filtered off, washed with methanol, diethyl ether and dried under vacuum. The product was purified by recrystallization from dichloromethane/petroleum ether (40–60 v/v) solvent system.

[(μ_2-2-pyridylaldazine)dichlorido*bis*(η^6-*p*-cymene)diruthenium(II)] tetraflouroborate: Orange microcrystalline solid. Yield: (1.404 g, 76%). *Anal. Calc*. for $B_2C_{32}Cl_2F_8H_{38}N_4Ru_2$; C, 41.54; H, 4.14; N, 6.05. *Found*: C, 41.16; H, 4.12; N, 5.97. ^{1}H NMR (500 MHz, DMSO-d_6): δ (ppm) = 9.71 (d, 2H, N = CH), 9.37 (s, 2H, $CH_{pyridyl}$), 8.67 (m, 2H, $CH_{pyridyl}$), 8.48 (td, 2H, $CH_{pyridyl}$), 8.06 (td, 2H, $CH_{pyridyl}$), 6.50 (d, 2H, CH_{phenyl}), 6.23 (br, 4H, CH_{phenyl}), 6.09 (br, 2H, CH_{phenyl}), 2.80 (m, 2H, $CH_{p\text{-}cymene}$), 2.31 (s, 6H, CH_3), 1.12 (m, 12H, $CH(CH_3)_2$). ^{13}C NMR (500 MHz, DMSO-d_6): δ (ppm) = 167.6 (N=C), 157.0 ($C_{pyridyl}$), 152.11 ($C_{pyridyl}$), 140.8 ($C_{pyridyl}$), 133.2 ($C_{pyridyl}$), 130.9 ($C_{pyridyl}$), 108.5 (C_{phenyl}), 87.5 (C_{phenyl}), 85.7 (C_{phenyl}), 83.8 (C_{phenyl}), 31.2 ($CH_{p\text{-}cymene}$), 22.9 (CH_3), 18.9 ($CH(CH_3)_2$). ESI-MS (TOF) (*m/z*): 801.96 {[(2-pyridylaldazine)$(C_{10}H_{14})_2Ru_2Cl_2BF_2]^+$ + H}; 481.99 {[(2-pyridylaldazine)$(C_{10}H_{14})$RuCl]$^+$ + H}; 270.97 [$(C_{10}H_{14})$RuCl]$^+$.

[(μ_2-*p*-phenylene*bis*(picoline)aldimine)dichlorido*bis*(η^6-*p*-cymene) diruthenium(II)] tetraflouroborate: Dark red crystalline solid. Yield: (1.378 g, 69%). *Anal. Calc*. for $B_2C_{38}Cl_2F_8H_{42}N_4Ru_2$; C, 45.58; H, 4.23; N, 5.59. *Found*: C, 45.82; H, 4.33; N, 5.50. ^{1}H NMR (500 MHz, DMSO-d_6): δ (ppm) = 9.64 (d, 2H, $CH_{pyridyl}$)), 9.04 (s, 2H, N = CH), 8.38 (t, 4H, $CH_{pyridyl}$)), 8.08 (d, 4H, CH_{phenyl}), 7.95–7.93 (m, 2H, $CH_{pyridyl}$), 6.19 (t, 2H, $CH_{phenyl\text{-}p\text{-}cymene}$), 5.87–5.84 (m, 2H, $CH_{phenyl\text{-}p\text{-}cymene}$), 5.77–5.71 (m, 4H, $CH_{phenyl\text{-}p\text{-}cymene}$), 2.61 (hept, 2H, $CH_{p\text{-}cymene}$), 2.23 (d, 6H, CH_3), 1.06 (m, 12H, $CH(CH_3)_2$). ^{13}C NMR (500 M Hz, DMSO-d_6): δ (ppm) = 169.2 (N=*C*), 156.6 ($C_{pyridyl}$), 154.9 ($C_{pyridyl}$), 152.8 ($C_{pyridyl}$), 140.6 (C_{phenyl}), 131.1 ($C_{pyridyl}$), 129.7 ($C_{pyridyl}$), 124.4 (C_{phenyl}), 106.0 ($C_{phenyl\text{-}p\text{-}cymene}$), 104.4 ($C_{phenyl\text{-}p\text{-}cymene}$), 87.1 ($C_{phenyl\text{-}p\text{-}cymene}$), 85.7 ($C_{phenyl\text{-}p\text{-}cymene}$), 31.0 ($CH_{p\text{-}cymene}$), 22.3 ($CH_3$), 18.9 ($CH(CH_3)_2$). ESI-MS (TOF) (*m/z*): 828.06 [(*p*-phenylene*bis*(picoline)aldimine)$(C_{10}H_{14})_2Ru_2Cl_2]^{2+}$; 557.05 [(*p*-phenylenebis(picoline)aldimine $(C_{10}H_{14})$RuCl]$^+$; 270.96 [$(C_{10}H_{14})$RuCl]$^+$.

[(μ_2-*p*-biphenylene*bis*(picoline)aldimine)dichlorido*bis*(η^6-*p*-cymene) diruthenium(II)] tetrafluoroborate: Brown red solid. Yield: (1.282 g, 59%) *Anal. Calc*. for $B_2C_{44}Cl_2F_8H_{46}N_4Ru_2$; C, 49.05; H, 4.30; N, 5.20. *Found*: C, 48.71; H, 4.34; N, 5.01. ^{1}H NMR (500 MHz, DMSO-d_6): δ (ppm) = 9.62 (d, 2H, $CH_{pyridyl}$), 9.02 (s, 2H, N = CH), 8.36–8.3 2 (m, 4H, $CH_{pyridyl}$), 8.14 (dd, 4H, CH_{phenyl}), 8.00 (d, 4H, CH_{phenyl}), 7.94 (t, 2H, $CH_{pyridyl}$), 6.15 (d, 2H, $CH_{phenyl\text{-}p\text{-}cymene}$), 5.83 (d, 2H, $CH_{phenyl\text{-}p\text{-}cymene}$), 5.74 (d, 2H, $CH_{phenyl\text{-}p\text{-}cymene}$), 5.66 (d, 2H, $CH_{phenyl\text{-}p\text{-}cymene}$), 2.60 (m, 2H, $CH_{p\text{-}cymene}$), 2.22 (s, 6H, CH_3), 1.05 (d, 12H, $CH(CH_3)_2$). ^{13}C NMR (500 MHz, DMSO-d_6): δ (ppm) = 168.3 (N=C), 156.5 ($C_{pyridyl}$), 155.0 ($C_{pyridyl}$),151.9 (C_{phenyl}), 140.5 ($C_{pyridyl}$), 130.7 ($C_{pyridyl}$), 129.5 ($C_{pyridyl}$), 128.3 (C_{phenyl}), 123.9 (C_{phenyl}), 105.7 (C_{phenyl}), 104.0 ($C_{phenyl\text{-}p\text{-}cymene}$), 87.1 ($C_{phenyl\text{-}p\text{-}cymene}$), 86.5 ($C_{phenyl\text{-}p\text{-}cymene}$), 85.6 ($C_{phenyl\text{-}p\text{-}cymene}$), 31.0 ($CH_{p\text{-}cymene}$), 22.3 ($CH_3$), 18.8 ($CH(CH_3)_2$). ESI-MS (TOF) (*m/z*): 905.01 {[(*p*-biphenylene*bis*(picoline)aldimine$(C_{10}H_{14})_2Ru_2Cl_2]^{2+}$ + H}; 634.15 { [(*p*-biphenylene*bis*(picoline) aldimine)$(C_{10}H_{14})$RuCl]$^+$ + H}; 270.99 $(C_{10}H_{14})$RuCl]$^+$.

[(μ_2-*p*-xylenebis(picoline)aldimine)dichlorido*bis*(η^6-*p*-cymene)diruthenium(II)] tetrafluoroborate: Orange solid. Yield: (1.692 g, 82%) *Anal. Calc*. for $B_2C_{40}Cl_2F_8H_{46}N_4Ru_2$; C, 46.67; H, 4.50; N, 5.44. *Found*: C, 46.36; H, 4.78; N, 5.38. ^{1}H NMR (500 MHz, DMSO-d_6): δ (ppm) = 9.54 (d, 2H, $CH_{pyridyl}$), 8.55 (s, 2H, N = CH), 8.26 (t, 2H, $CH_{pyridyl}$), 8.17 (d, 2H, b$CH_{pyridyl}$), 7.83 (t, 2H, $CH_{pyridyl}$), 7.59 (s, 4H, CH_{pheny}), 6.25 (d, 2H, $CH_{phenyl\text{-}p\text{-}cymene}$), 6.13 (d, 2H, $CH_{phenyl\text{-}p\text{-}cymene}$), 5.93–5.88 (m, 4H, CH_2), 5.75 (d, 2H, $CH_{phenyl\text{-}p\text{-}cymene}$), 5.56 (d, 2H, $CH_{phenyl\text{-}p\text{-}cymene}$), 2.61 (m, 2H, $CH_{p\text{-}cymene}$), 2.11 (s, 6H, CH_3), 1.02 (d, 6H, $CH(CH_3)$), 0.94 (d, 6H, $CH(CH_3)$). ^{13}C NMR (500 MHz, DMSO-d_6): δ (ppm) = 167.9 (N=C), 156.4 ($C_{pyridyl}$), 154.8 ($C_{pyridyl}$), 140.2 ($C_{pyridyl}$), 135.2 ($C_{pyridyl}$), 131.0 (C_{phenyl}), 129.7 (C_{phenyl}), 128.8 ($C_{pyridyl}$), 105.0 ($C_{phenyl\text{-}p\text{-}cymene}$), 103.9 ($C_{phenyl\text{-}p\text{-}cymene}$), 87.9 ($C_{phenyl\text{-}pcymene}$), 84.5 ($C_{phenyl\text{-}p\text{-}cymene}$), 68.9 ($CH_2$), 30.9 ($CH_{p\text{-}cymene}$), 21.9($CH_3$), 18.8 ($CH(CH_3)_2$). ESI-MS (TOF) (*m/z*): 904.96 [(*p*-xylenebis(picoline)aldimine) $(C_{10}H_{14})_2Ru_2Cl_2BF_2]^+$; 585.13 [(*p*-xylene*bis*(picoline)aldimine) $(C_{10}H_{14})$RuCl]$^+$; 270.99 [$(C_{10}H_{14})$RuCl]$^+$.

2.5. Aquation of the complexes

The chlorido complexes were converted into their respective aqua complexes (Ru-1; Ru-2; Ru-3 and Ru-4). In a typical reaction, 1.00 mmol of the chlorido complex was reacted with 1.99 mmols of $AgClO_4$ in 0.01 M $HClO_4$. In all the reactions, the mixtures were stirred in the dark at 50 °C for 48 h. The solutions were thereafter cooled to ambient temperature, allowed to stand for at least 3 h and the grey AgCl precipitate filtered off using 0.45 μm nylon membrane [20]. The filtrates were diluted appropriately for p*K*a titrations and kinetic studies.

2.6. Determination of pKa of the aqua complexes

Spectrophotometric acid-base titration of the aqua complexes with NaOH was done from pH 2 to 12 at 25 °C. Large complex volumes (about 500 mL) were used to avoid dilution effects and absorbance corrections [21]. Within pH 2–3, small grains of crushed NaOH pellets were added while beyond pH 3, dilute NaOH solutions were added drop-wise using a Pasteur pipette. The titrations were done in such a way that many evenly distributed points were obtained. After each base addition, the complex solution was stirred for about 2 min prior to pH measurement and respective spectrum acquisition. For the pH measurements, about 0.6 mL aliquots in glass ampules were used and discarded to avoid contamination of the stock complex solution with chloride ions from the electrode while the aliquots used for absorbance measurements were returned back to the stock solution. A confirmatory reverse pH titration was done using $HClO_4$ solutions in place of NaOH. During the pH reverse titration the baseline and isosbestic points remained intact, which compares favourably with similar spectrometric titrations of binuclear platinum(II) complexes reported in literature [9].

2.7. Kinetic measurements

Nucleophile solutions of known concentration maintained at pH 2.0 and 0.1 M $HClO_4/NaClO_4$ ionic strength were prepared shortly before use. Likewise, the solutions of the aqua ruthenium(II) complexes solutions were maintained at similar pH and ionic strength. Their concentrations were; Ru-1 (0.248 mM), Ru-2 (0.660 mM), Ru-3 (0.144 mM), Ru-4 (0.171 mM). Substitution reactions were performed under *pseudo*-first order conditions in which the nucleophilic concentration was at least 40 folds higher than the concentration of the metal complex to drive the reactions to completion. The reactions were initiated by mixing equal volumes of thermally equilibrated complex and nucleophile in a tandem cuvette. The ultraviolet–visible spectral changes resulting from the reactions were recorded from 800 to 200 nm wavelength range. Concentration dependence studies were performed at a constant temperature of 25 °C. On the other hand, temperature dependence of reaction rates was studied from 25 to 45 °C at an interval of 5 °C. To establish whether there were other reactions beyond the first step, all reactions were left to proceed for some time after their completion. The convergence of absorbance values after the first step signified the absence of other reactions. For each reaction, at least three independent runs were performed.

2.8. Computational modelling

Computational calculations were performed using density functional theory (DFT) method implemented by Gaussian 09 W suite of programs [22]. The structures were optimized using the hybrid Becke,

3-parameter, Lee-yang-Parr at the standard Los Alamos National Laboratory 2 double ζ (LANL2DZ) basis set [23]. DFT utilizes electron density over wave-function in the determination of a system's properties. Therefore, it is applicable in these complexes with large number of electrons since electron densities are always three dimensional irrespective of the number of electrons involved [24]. LANL2DZ exploits relativistic effective core potentials to effectively account for the inner core 28 electrons ($[Ar]3d^{10}$) in ruthenium [25]. The systems were fully optimized in aqua media using conductor-like polarizable continuum solvent model [26] at singlet spin ground state and an overall charge of +4. For comparison purposes, the respective mononuclear congeners were optimized like the binuclear complexes except that their overall charge was set at +2.

Quantum chemical descriptors; chemical hardness (η), chemical softness (σ) and global electrophilicity indices (ω) for the complexes were calculated as described in literature [27–30]. Due to its high reliability Hirshfeld population analysis was used to determine the atomic charges in the complexes [31,32].

3. Results

3.1. Acid-Base equilibria of the aqua complexes

p*K*a values of the complexes were determined by fitting Boltzmann sigmoid function on the plot of absorbance versus pH at a selected wavelength. Typical ultraviolet–visible spectra obtained for the titration of Ru-1 with NaOH is presented in Fig. 2. The inset shows a plot of absorbance as a function of pH at λ = 290 nm. The p*K*a values obtained are collected in Table 1. Additional plots are presented in the Supplementary Information (Figures SI 5–6)

Complexes Ru-1, Ru-2 and Ru-3, displayed a stepwise deprotonation of the aqua ligands, recording a positive relationship between the p*K*a values and the length of the linker. As the separation distance increases, the charge addition between the two metal centres decreases, thus decreasing the electrophilicity of the complexes and acidity of the coordinated aqua ligands [9,33]. For instance; the short Ru-Ru intermetallic distance in Ru-1 enables effective electronic communication between the two metal centres, leading to an overall high acidity of the bound aqua ligands. The pKa_2 values obtained are at least 0.9 p*K*a units more basic than pKa_1. This is because after the deprotonation of the first aqua ligand, the overall charge of the complex reduces from +4 to +3 making the second metal center less electrophilic hence diminishing the tendency for another deprotonation to occur [8,12,34]. A similar observation has been made on binuclear ruthenium(II) complexes and binuclear platinum(II) complexes [14,35,36]. In these reported studies the p*K*a values increased with decrease in π-acceptor ability of the bridging ligand as well as increase in the donor ability of the bridging ligand. The stepwise deprotonation of the aqua ligands is illustrated in Scheme 1.

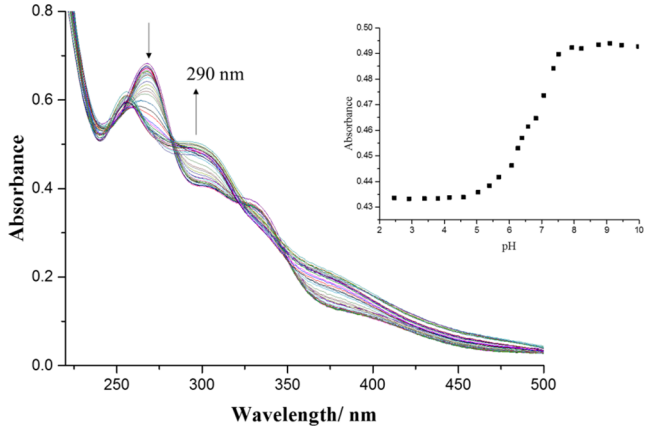

Fig. 2. Ultraviolet–visible spectra of Ru-1 recorded as a function of pH (2–10) at 298 K. Inset: A plot of absorbance versus pH at λ = 290 nm.

Table 1
Summary of pKa values obtained for the deprotonation of the aqua ligands.

Complex	Ru-1	Ru-2	Ru-3	Ru-4
pKa_1	6.32 ± 0.12	6.76 ± 0.03	6.85 ± 0.05	6.97 ± 0.02
pKa_2	7.23 ± 0.04	8.98 ± 0.03	10.71 ± 0.04	–

A single p*K*a value was observed in complex Ru-4, signaling simultaneous deprotonation of the coordinated aqua ligands. The simultaneous deprotonation in Ru-4 is illustrated in Scheme 2.

The *p*-xylene*bis*(picoline)aldimine bridging ligand in Ru-4 is unconjugated beyond the α,α′-diimines, this causes weak interactions between the metal centres making them act independently [9,16]. The single p*K*a value obtained is supported by electrochemical reduction of a complex utilizing this ligand which showed a single broad two-electron reduction wave [16]. Compared to the pKa_1 values of other complexes, the high value obtained in Ru-4 is attributed to the methylene groups which lower the localized charge on the metal centres through inductive σ-donation [37]. As a result the basicity of the coordinated aqua ligands is enhanced. A single p*K*a value has also been reported for binuclear platinum(II) complexes [9,38]. For both the stepwise (for complexes Ru-1 to Ru-3) and simultaneous (for Ru-4) deprotonation processes, two equivalents of OH^- were consumed as illustrated in Scheme 1 and 2, respectively [39].

From the acidity constants, all the complexes exist exclusively as aqua species at a pH of 2.0. Considering this, all the kinetic studies were performed at pH 2.0.

3.2. Computational results

Computational modelling was carried out to gain an insight on the spatial arrangement of the ligand systems as well as electronic properties of the complexes. Geometry optimized structures of the complexes and their respective frontier orbitals are shown in Fig. 3 while key computational results obtained are documented in Table 2. Table SI 9 (Supplementary Information) summarizes key computational results obtained for the mononuclear analogues of the studied complexes. Fig. 4 shows typical numbering of the nitrogen atoms in the complexes.

From the mappings of the frontier orbitals, it is observed that the HOMO in Ru-1 is largely based on the metal centres and arene ligands. In Ru-2 and Ru-3, it is spread throughout the complex with the phenyl and biphenyl spacers making substantial contributions. In Ru-4, the HOMO is largely concentrated on one of the two Ru-α,α′-diimine moieties and the proximate arene group. This shows that there is a weak interaction between the two metal centres in the complex [40]. The single pKa value observed in Ru-4 support this proposition as explained *vide supra*. On the other hand, the LUMO is largely based on the bridging ligand for all complexes.

The planarity of the minimum energy structures obtained, shows that the two 9-atomic Ru-α,α′-diimine moieties are non-planar to one another in all the complexes (Figure SI 7–10). In complexes Ru-1 and Ru-3, the two moieties are tilted away from each other at a dihedral angle of 5.33° and 33.08°, respectively. In Ru-3 the phenyl rings in the bridging ligand are twisted away from the mean plane of whole bridging ligand at an angle of 47.01 °, as a result of steric interactions between imine protons and proximate protons on the biphenyl spacer. In addition, the two phenyl rings are twisted in opposite direction to one another at an average angle of 30.27°. This is attributed to steric interactions between the proximate hydrogen atoms on the phenyl rings [41]. These angles are shown in Figures SI 11 and 12.

In Ru-2 the phenyl spacer binds the two 9-atomic Ru-α,α′-diimine moieties in way that their planes are parallel but separated by a minute separation distance of 0.446 Å. The minute separation distance is

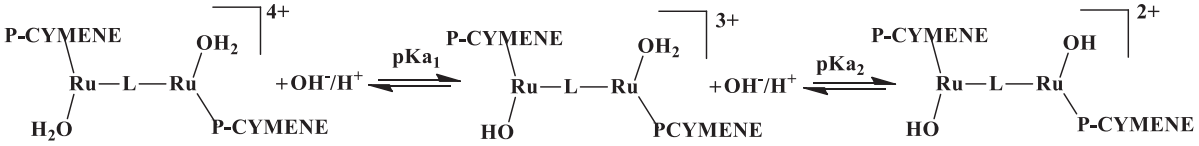

Scheme 1. Stepwise deprotonation of the aqua ligands in complexes Ru-1-Ru-3.

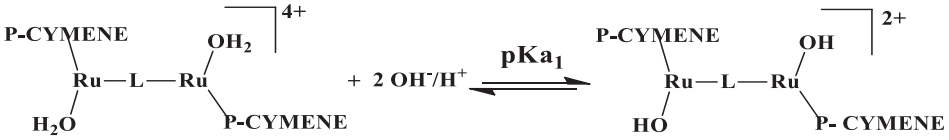

Scheme 2. Simultaneous deprotonation of the aqua ligands in complex Ru-4.

attributed to high rigidity of the bridging ligand therein [16]. The phenyl spacer in Ru-2 lies out of the plane of the whole bridging ligand at an angle of 46.26° because of steric interactions of hydrogen atoms on the spacer and that of imine groups [41]. The crystal structure of the chlorido analogue of Ru-2 exhibit similar structural behavior [18].

The two planes in Ru-4 are parallel to one another with a huge separation distance of 5.473 Å (Figure SI 10). This humongous separation distance is attributed to the high flexibility of the ligand therein. The bridging ligand in Ru-4 form two V-shaped curvatures of average angle of 112.18° as shown in Fig. 5. This is attributed to the presence of methylene groups which enhances the flexibility of the bridging ligand.

The Ru-N1 bond length is invariant across the complexes, denoting that the spacer does not affect electronic distribution in the pyridyl moieties of the complexes. Similarly for their mononuclear congeners, the Ru-N1 bond length remained invariant (refer to Table SI 9). On the contrary, the linker influences the Ru-N2 and Ru-OH_2 bond lengths. The shortening of Ru-N2 and elongation of Ru-OH_2 bond from Ru-1 to Ru-4, shows progressive increase in the σ-donor ability of the spacers [9]. The Ru-OH_2 bonds in the mononuclear complexes are slightly longer than in the binuclear complexes. Unlike in the mononuclear complexes, the electron density of the bridging ligand is shared between the metal centres of the binuclear complexes. As a result, the repulsion of electron clouds between the metal centre and the aqua ligand is higher in the mononuclear complexes [33]. This is supported by the lower atomic charges on the ruthenium metal centers. As an example, the charge on ruthenium metal centre in Ru-1 is 0.128 compared to 0.102 on the

Table 2
Key computational data for the optimized complexes.

Complex	Ru-1	Ru-2	Ru-3	Ru-4
HOMO-LUMO energies / eV				
HOMO	−7.335	−7.038	−6.885	−7.129
LUMO	−4.318	−3.772	−3.598	−3.409
$\Delta E_{HOMO-LUMO}$	3.017	3.266	3.287	3.720
Chemical hardness (η) / eV	1.509	1.633	1.644	1.860
Chemical softness (σ) / eV^{-1}	0.663	0.612	0.608	0.538
Electrophilicity index (ω) / Ev	11.252	8.945	8.358	7.463
Hirshfeld charge (Ru)	0.128	0.121	0.117	0.109
Bond Length / Å				
Ru-N2	2.146	2.090	2.088	2.083
Ru-N1	2.076	2.077	2.077	2.078
Ru-OH_2	2.148	2.152	2.154	2.157
Ru-Ru	5.314	8.783	12.873	
Diimine moiety planes separation / Å	–	0.446	–	5.473
Dihedral angle of diimine moiety planes /°	5.33	–	33.08	–

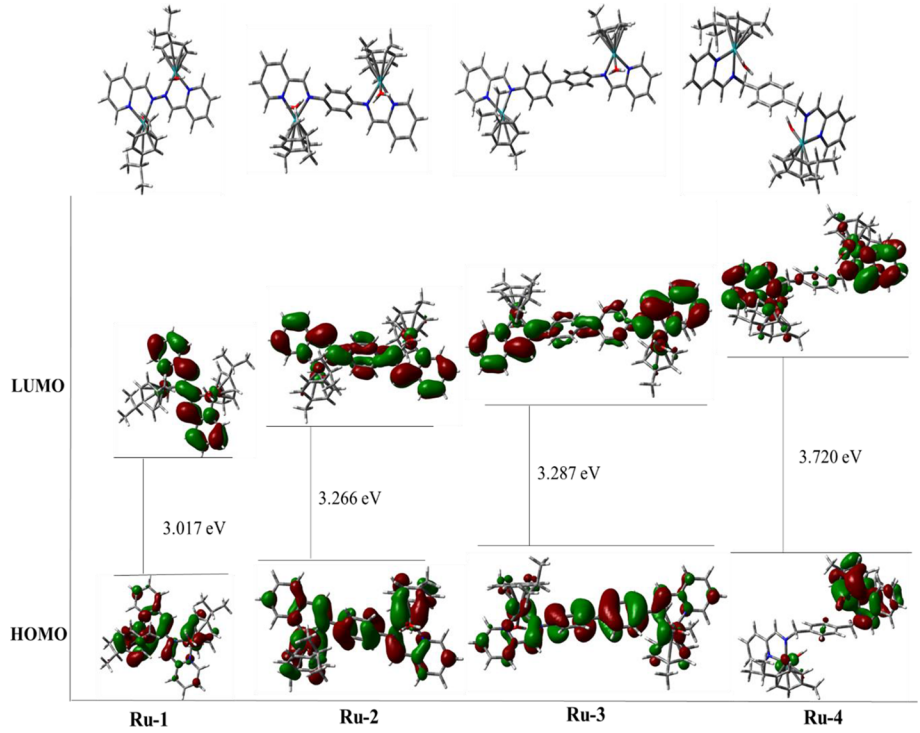

Fig. 3. Geometry optimized structures, frontier orbitals and their respective energy gaps for the studied complexes.

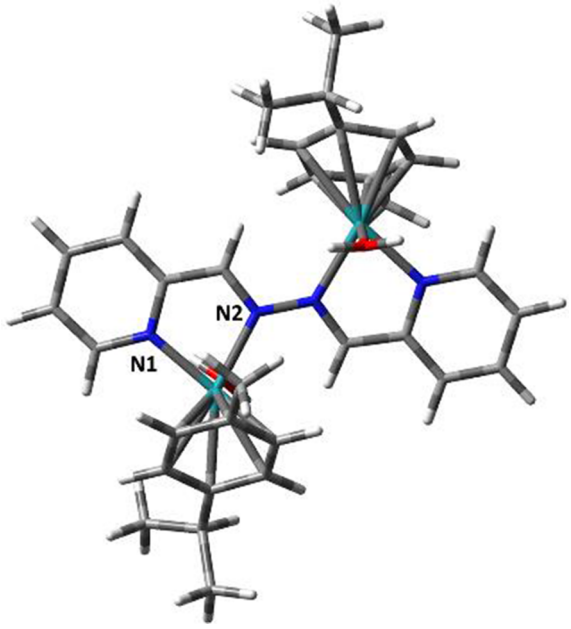

Fig. 4. DFT-optimized structure showing numbering of the nitrogen atoms in the complexes.

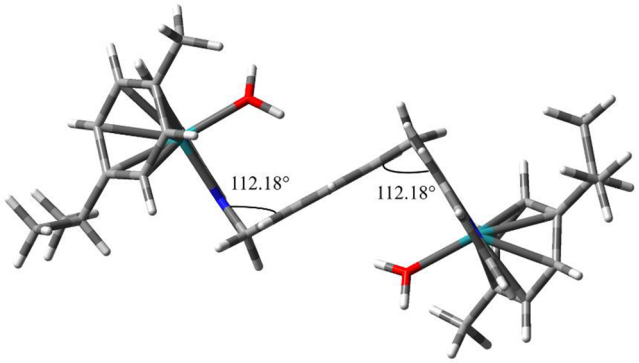

Fig. 5. Geometry optimized structure of Ru-4 showing the V-shaped curvatures.

metal centre of its mononuclear analogue.

Inspection of the quantum chemical descriptors documented in Table 2, show that the LUMO energy shifts proportionately to more positive values as the linker is varied from 2-pyridyl aldazine to *p*-xylene*bis*(picoline)aldimine. Likewise, from Ru-1 to Ru-4, the HOMO-LUMO gap increase with concomitant decrease in the electrophilicity indices of the complexes and localized charge on the ruthenium atoms (refer to the trend in the Hirshfeld charges). The increase in chemical hardness/decrease in chemical softness from Ru-1 to Ru-4, point out to an increase in the stability of the complexes as the bridging ligand is varied from 2-pyridylaldazine to *p*-xylene*bis*(picoline)aldimine [42]. As documented in Table SI 9, the quantum chemical descriptors in the mononuclear complexes followed the same trend as the binuclear complexes, differing only on their magnitude. The energy gap between the frontier molecular orbitals is larger in the mononuclear complexes compared to the binuclear complexes thus making the former set of complexes more stable [42]. Consequently, they are predicted to be less reactive than the binuclear complexes. This further supported by their lower global electrophilicty indices and chemical softness and higher chemical hardness [13,29,42]. Similar observations have been made on platinum(II) complexes [13].

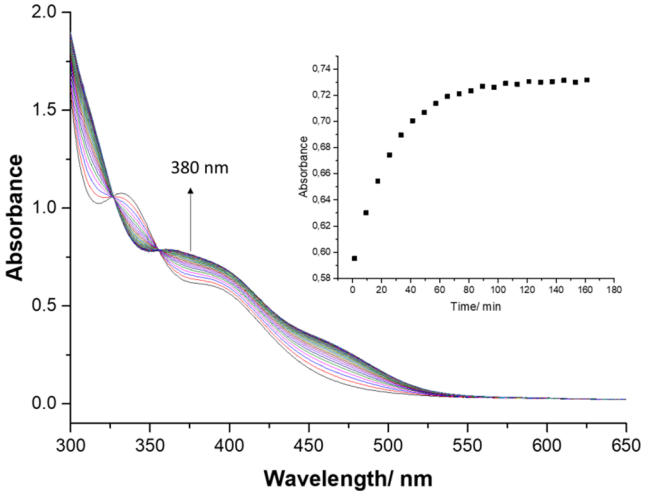

Fig. 6. Ultraviolet–visible spectra for the reaction of Ru-4 (0.17 mM) with Dmtu (34.2 mM) at 298 K, pH = 2.0, I = 0.1 M $HClO_4/NaClO_4$. Inset: A kinetic trace obtained at λ = 380 nm.

3.3. Kinetic results

The rate of displacement of the coordinated aqua ligands in the four complexes were investigated using thiourea based nucleophiles of varied steric demands under *pseudo*-first order conditions. The substitution reactions were monitored spectrophotometrically by following change in absorbance of the spectra at a selected wavelength as a function of time. Typical spectra obtained for the reaction of Ru-4 with Dmtu at 25 °C is shown Fig. 6.

The kinetic traces taken at the suitable wavelength were fitted into a single exponential decay standard function to generate *pseudo*-first order rate constants (k_{obs}) using equation (i) [43].

$$A_t = A_o + (A_o - A_\psi)\exp(-k_{obs}t) \quad \text{(i)}$$

where; A_o = absorbance at the initiation of the reaction, A_t = absorbance at time t, and A_∞ = absorbance at the end of the reaction.

The k_{obs} values obtained were plotted against nucleophile concentrations. A linear dependence of k_{obs} on the nucleophile concentration was exhibited by all the reactions of the complexes. The intercept of all the plots was zero, indicating the absence of reverse or solvolysis reaction. A collection of k_{obs} values and respective nucleophile concentrations are presented in the Supplementary Information (Tables SI 1–4). Typical plots of k_{obs} versus nucleophile concentration obtained for Ru-4 is shown in Fig. 7. Additional plots are presented in the Supplementary Information (Figures SI 1–2). The second order rate constant (k_2) for the reactions was obtained from the slopes of the plots. The values obtained are tabulated in Table 3. All the concentration dependent substitution reactions can be described by the equation (ii).

$$k_{obs} = k_2[Nucleophile] \quad \text{(ii)}$$

To determine the thermodynamic parameters of the substitution process, the reaction temperature was varied systematically from 25 °C to 45 °C at an interval of 5 °C and the respective temperature dependent k_2 calculated. The $\ln(k_2/T)$ values obtained were plotted as a function of 1/T. Activation enthalpy ($\Delta H^{\neq}$) and entropy ($\Delta S^{\neq}$) were calculated from the slope and the y-intercept, respectively using the Eyring equation (iii) [43].

$$ln(k_2/T) = -\Delta H^{\neq}/RT + (23.78 + \Delta S^{\neq}/R) \quad \text{(iii)}$$

Typical Eyring plots obtained for Ru-4 are shown in Fig. 8 and the values of $\Delta H^{\neq}$ and $\Delta S^{\neq}$ obtained are given in Table 3. Additional

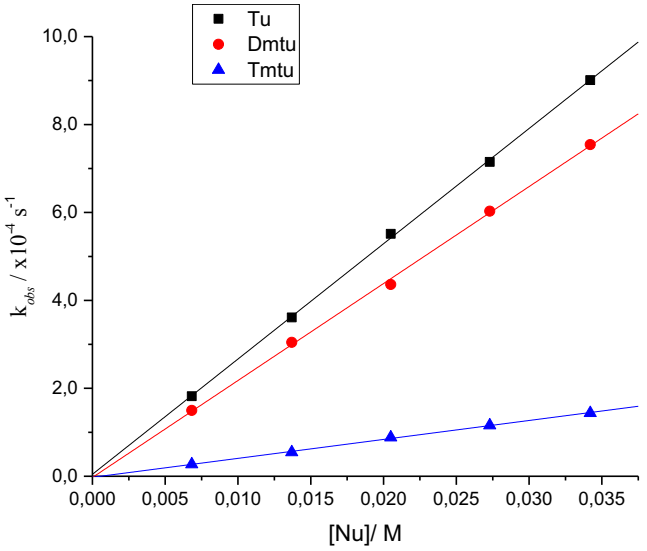

Fig. 7. Dependence of pseudo-first order rate constant (k_{obs}) on the concentration of thiourea nucleophiles for the substitution of the aqua ligands in Ru-4 at 25 °C, pH = 2.0, I = 0.1 M $HClO_4/NaClO_4$.

Table 3
Summary of second order rate constants (k_2) at 25 °C and activation parameters.

Complex	Nu	k_2 /10^{-3} M^{-1} s^{-1}	$\Delta H^{\neq}$ /kJmol^{-1}	$\Delta S^{\neq}$ /Jmol^{-1}K^{-1}
Ru-1	Tu	84.2 ± 0.8	59 ± 2	−68 ± 7
	Dmtu	60.8 ± 0.5	57 ± 1	−77 ± 4
	Tmtu	16.3 ± 0.4	64 ± 1	−65 ± 4
Ru-2	Tu	2.20 ± 0.03	60 ± 2	−95 ± 5
	Dmtu	2.89 ± 0.04	59 ± 2	−97 ± 5
	Tmtu	1.21 ± 0.01	66 ± 2	−78 ± 5
Ru-3	Tu	4.99 ± 0.03	62 ± 2	−80 ± 5
	Dmtu	5.41 ± 0.05	66 ± 1	−68 ± 4
	Tmtu	1.72 ± 0.03	70 ± 2	−62 ± 5
Ru-4	Tu	26.4 ± 0.1	59 ± 2	−69 ± 8
	Dmtu	22.0 ± 0.2	63 ± 2	−64 ± 5
	Tmtu	4.21 ± 0.04	78 ± 2	−29 ± 5

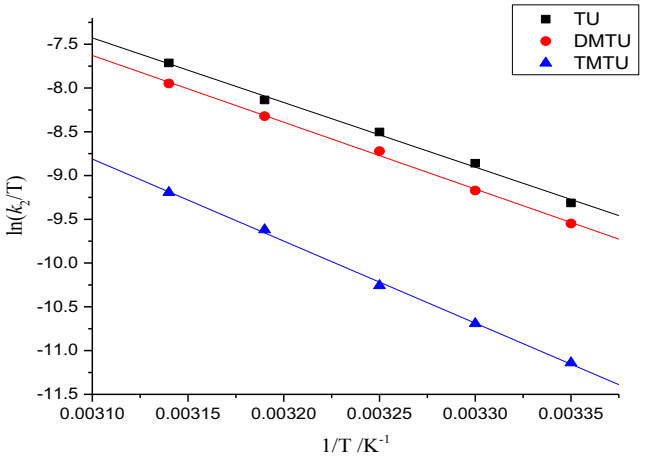

Fig. 8. Eyring plots for the reaction of Ru-4 with thiourea nucleophiles in the range 25–45 °C, pH = 2.0, I = 0.1 M $HClO_4/NaClO_4$.

Eyring plots and values of ln(k_2/T) and respective 1/T are presented in the Supplementary Information (Figure SI 3–4 and Table SI 5–8).

4. Discussion

In this study, the effect of α,α′-diimine-based bridging ligands on the reactivity of low-spin d^6 binuclear ruthenium(II) *para*-cymene complexes was investigated. The bridging ligand binds the metal centres forming two 5-membered stable chelate rings. The electron donating aliphatic substituents on the *para*-cymene ligand fortify the Ru-*para*-cymene bonds, making the *para*-cymene ligand unfavorable to substitution [44]. In all the complexes, a single substitution step was observed, indicating that the two coordinated aqua ligands were simultaneously displaced by the thiourea nucleophiles. With Tu as the entering group, the k_2 values decreased in the order; Ru-1 (0.084 $M^{-1}s^{-1}$) > Ru-4 (0.026 $M^{-1}s^{-1}$) > Ru-3 (0.005 $M^{-1}s^{-1}$) > Ru-2 (0.002 $M^{-1}s^{-1}$). Similarly, the other two nucleophiles followed the same trend. The differences in reactivity observed is attributed to stereo-electronic properties brought about by the coordinated bridging ligand.

A comparison of reactivity referenced to Ru-1 shows that this complex is at least 3 times more reactive than the other complexes. This is attributed to its strong π-acceptor 2-pyridylaldazine bridging ligand [16,45]. This is evident from the computational results which show that the frontier molecular orbitals are well stabilized and the energy gap between them is narrower compared to the rest of the complexes. Therefore, Ru-1 is more electrophilic due to effective π-back-donation from the dπ orbitals largely based on metal ion to the stabilized π* orbital of the bridging ligand [21]. Moreover, the short Ru-Ru intermetallic distance (5.314 Å) in Ru-1 promotes effective electronic communication between the metal centres, thus strengthening the π-back-bonding effects through enhanced electron density delocalization [45]. The metal centres are thus deprived of electron density making them more positively charged as shown by a large Hirshfeld charge of 0.128. This makes them more attractive for facile nucleophilic attack. The low p*K*a values in Ru-1, documented corroborate this argument, refer to Table 1.

When spacers; phenyl (Ru-2), biphenyl (Ru-3) and xylyl (Ru-4) are placed between α,α′-diimine moieties, the complexes become progressively less electrophilic because of destabilization of the LUMO orbitals with concomitant widening of the HOMO-LUMO energy gap [46]. This reduces the ability of the bridging ligand to withdraw electrons from the metal centres as indicated by the diminution of the local charges on the metal centres from Ru-1 to Ru-4. As shown by the modelled structures, the bridging ligands in Ru-2, Ru-3 and Ru-4 are distorted. For instance; the phenyl ring(s) in Ru-2 and Ru-3 are twisted out of the mean plane of the bridging ligand at a dihedral angles of 46.26° and 47.01°, respectively. These distortions further compromise the π-acceptor abilities of the bridging ligands, hence reducing the electrophilicity of the complexes [47].

The observed differences in quantum chemical descriptors as the linker is varied is validated by preceding studies utilizing these ligands [16,48]. Characteristic metal to ligand charge transfer ($t_2g \rightarrow \pi^*$) bands show a hypsochromic shift as the bridging ligand is changed from 2-pyridylaldazine (Ru-1) to *p*-xylene*bis*(picoline)aldimine (Ru-4). This signals an increase in the HOMO-LUMO gap and therefore the energy required to effect electronic promotion increases accordingly. Likewise, the reduction potentials of related complexes show a consistent shift to more negative values as the ligand is varied from 2-pyridylaldazine to *p*-xylene-bis(picoline)aldimine as result of the destabilization of the π* LUMO orbitals. Therefore, the electron withdrawing ability of the ligands decreases from 2-pyridylaldazine to *p*-xylene*bis*(picoline)aldimine. This would lead the reactivity to decrease from Ru-2 to Ru-4. However, the opposite trend was observed and this is due to a progressive decrease in steric hindrance in the vicinity of the metal centres as the bridging ligand is varied from *p*-phenylenebis(picoline)aldimine to *p*-xylene*bis*(picoline)aldimine [8,49]. A change of the bridge from Ru-2 to Ru-4 restricts the metal centres of the latter complexes to geometric orientations that reduce the steric congestion around the metal centres. This is demonstrated by the variance in the non-planarity topography of the two Ru-α,α′-diimine moieties for the complexes. The metal centres in Ru-2 are the most sterically hindered by the bridging

ligand and the arene groups. This is due to its relatively short Ru-Ru intermetallic distance (8.783 Å) and the limited ability of the bridging ligand to rotate as shown by the minute inter-plane distance (0.446 Å) between the planes of the Ru-α,α′-diimine moiety [32]. As the spacer is changed from phenyl (Ru-2) to biphenyl (Ru-3), the distance between the metal centres increases of the latter to 12.873 Å and the flexibility of the bridging ligand slightly increases [50]. This causes the two Ru-α,α′-diimine moieties to tilt away from each other at a dihedral angle of 33.08°. As a result, the steric hindrance around the metal centres is alleviated, making the metal centres more exposed for nucleophilic attack.

When compared to Ru-2 and Ru-3, incoming nucleophiles experience less steric hindrance in attacking the metal centres in Ru-1. This is because of the absence of a spacer between the azine nitrogen atoms in Ru-1 unlike in Ru-2 and Ru-3. Importantly, Ru-1 has a rotational freedom around the N−N single bond that further alleviates possible steric hindrance, while in Ru-2 and Ru-3 such possibility is minimal due to increased rigidity of the bridging ligands therein [18].

In Ru-4, due to the high flexibility of the bridging ligand, the metal centres are aligned along two parallel vectors resulting in a large separation distance (5.473 Å) between the planes of the Ru-α,α′-diimine moieties. This significantly reduces the steric shielding around the metal centres, making them more accessible for nucleophilic attack. Furthermore, its optimized structure (Fig. 5) suggest a solvent assisted entrapment of the incoming nucleophiles through the cage effect at its proximate V-shaped cavities [51]. The entrapped molecules promote effective collisions with the metal centres thereby enhancing the reactivity of the complex. The cage effect has been reported to enhance the reactivity of binuclear platinum complexes [8,9].

A look at the Ru-OH_2 bond lengths show an increasing trend from Ru-1 to Ru-4. Contrary to this, is the variation in the Hirshfeld charges on the metal centres which show a decreasing trend. Both trends are due to progressive increase in electron density at the metal centres through inductive donation from the spacers [33]. Therefore, the *trans*-influence of the xylyl spacer as depicted by the elongated Ru-OH_2 bond and the markedly low atomic charge on the ruthenium centres in Ru-4 makes the substitution of the aqua ligands in Ru-4 easier compared to Ru-3 and Ru-2 [8,33].

Further, the trend of reactivity for these binuclear complexes is in agreement with those reported from other studies which have shown that increase in steric hindrance caused by the chelating ligand decrease the reactivity of arene ruthenium(II) complexes [14,52,53].

It is expected that, the reactivity of the three nucleophiles should follow the trend Tu > Dmtu > Tmtu due to increasing bulkiness of the nucleophiles. However, in Ru-2 and Ru-3, the more sterically hindered Dmtu reacts faster that Tu. This is due to inductive effect brought about by the two methyl substituents in Dmtu which donate electron density to the sulfur atom increasing the nucleophilicity of the nucleophile [21,54]. For Tmtu, the four methyl substituents retards its approach towards the metal centres, causing a transition state destabilization leading to high activation enthalpy which slows down the reactivity [55].

The negative values of $\Delta S^{\neq}$ and the low positive values of $\Delta H^{\neq}$ suggest an associative mechanism of activation [43]. The negative activation entropy also imply a more ordered transition state compared to the starting conditions and the final products [56]. An associative mechanism of activation has also been reported in other arene-based ruthenium(II) complexes [14,52,57].

5. Conclusions

The present study has demonstrated that the reactivity of binuclear ruthenium(II) *p*-cymene complexes with α,α′-diimine bridging ligands is controlled by the inherent steric and electronic factors associated with the bridging ligand. The high reactivity in Ru-1 compared to the other complexes is ascribed to the strong π-acceptor properties of 2-pyridylaldazine bridging ligand which enhances the electrophilicity of the complex, hence making the metal centres more attractive for facile nucleophilic attack. The other complexes have electron donor spacers between the azine nitrogen atoms of their bridging ligands which compromise their π-acceptor properties, thus lowering their electrophilicity. This is supported by the computational results which indicate that the HOMO-LUMO gap and chemical hardness are least in Ru-1 and increase progressively from Ru-2 to Ru-4. Furthermore, the coordinated aqua ligands in Ru-1 are the most acidic as indicated by the lowest stepwise p*K*a values. Therefore, the metal centres in Ru-1 are more attractive for nucleophilic attack than in the other complexes. In complexes Ru-2, Ru-3 and Ru-4, the reactivity is inversely correlated to the steric hindrance in the vicinity of the metal centres. Increased flexibility of the ligand reduces steric congestion around the metal centre hence increasing the reactivity of the complexes. In Ru-4, the presence of the two V-shaped curvatures proximate to the metal centres facilitate entrapment of the incoming nucleophile through the cage effect, leading to more effective collisions with the metal centres. The reactions proceed through an associative mechanism.

Funding

This research was funded by the University of KwaZulu-Natal, South Africa.

Declaration of Competing Interest

The authors declare that they have no known competing financial interests or personal relationships that could have appeared to influence the work reported in this paper.

Acknowledgements

The authors gratefully acknowledge the University of KwaZulu-Natal, South Africa and Masinde Muliro University of Science and Technology, Kenya for their financial support. We are grateful to Mr. Craig Grimmer and Mrs. Caryl Janse van Rensburg for their assistance in characterization of the ligands and complexes.

Appendix A. Supplementary data

Supplementary data to this article can be found online at https://doi.org/10.1016/j.ica.2020.119972.

References

[1] P. Kumar, R.K. Gupta, D.S. Pandey, Chem. Soc. Rev. 43 (2014) 707–733, https://doi.org/10.1039/c3cs60189g.
[2] M.V. Babak, W.H. Ang, Met. Ions Life Sci. 18 (2018) 171–198, https://doi.org/10.1515/9783110470734-012.
[3] Y.K. Yan, M. Melchart, A. Habtemariam, P.J. Sadler, Chem. Commun. (2005) 4764–4776, https://doi.org/10.1039/b508531b.
[4] G. Li, D. Zhu, X. Wang, Z. Su, M.R. Bryce, Chem. Soc. Rev. 49 (2020) 765–838, https://doi.org/10.1039/c8cs00660a.
[5] H. Chen, J.A. Parkinson, O. Nováková, J. Bella, F. Wang, A. Dawson, R. Gould, S. Parsons, V. Brabec, P.J. Sadler, Proc. Natl. Acad. Sci. U.S.A. 100 (2003) 14623–14628, https://doi.org/10.1073/pnas.2434016100.
[6] S.D. Brown, K.D. Trotter, O.B. Sutcliffe, J.A. Plumb, B. Waddell, N.E. Briggs, N.J. Wheate, Dalton Trans. 41 (2012) 11330–11339, https://doi.org/10.1039/c2dt31313h.
[7] H. Rogers, S. Arachchige, K. Brewer, S. Swavey, Compre. Coord. Chem. II (1) (2003) 135–157, https://doi.org/10.1016/B978-0-12-409547-2.11314-9.
[8] A. Mambanda, D. Jaganyi, Dalton Trans. 41 (2012) 908–920, https://doi.org/10.1039/c1dt11516b.
[9] A. Mambanda, D. Jaganyi, S. Hochreuther, R. van Eldik, Dalton Trans. 39 (2010) 3595–3608, https://doi.org/10.1039/b921687a.
[10] H. Ertürk, A. Hofmann, R. Puchta, R. van Eldik, Dalton Trans. (2007) 2295–2301, https://doi.org/10.1039/b700770c.
[11] P.A. Wangoli, G. Kinunda, New J. Chem. 42 (2018) 214–227, https://doi.org/10.1039/c7nj03021e.
[12] T. Soldatović, S. Jovanović, Ž.D. Bugarčić, R. van Eldik, Dalton Trans. (2007)

2295–2301, https://doi.org/10.1039/b700770c.
[13] A. Shaira, D. Jaganyi, J. Coord. Chem. 68 (2015) 3013–3031, https://doi.org/10.1080/00958972.2015.1064114.
[14] G.K. Mutua, R. Bellam, D. Jaganyi, A. Mambanda, J. Coord. Chem. 72 (2019) 2931–2956, https://doi.org/10.1080/00958972.2019.1676893.
[15] W.C. Schiessl, N.K. Summa, C.F. Weber, S. Gubo, C. Dücker-Benfer, R. Puchta, N.J. van Eikema Hommes, R. van Eldik, Z. Anorg. Allg. Chem., 631 (2005) 2812-2819. https://doi.org/10.1002/zaac.200500157.
[16] M.-A. Haga, K. Koizumi, Inorg. Chim. Acta. 104 (1985) 47–50, https://doi.org/10.1016/S0020-1693(00)83784-6.
[17] D.A. Edwards, G.M. Hoskins, M.F. Mahon, K.C. Malloy, G.R. Rudolph, Polyhedron 17 (1998) 2321–2326, https://doi.org/10.1016/S0277-5387(97)00533-0.
[18] A. Singh, M. Chandra, A.N. Sahay, D.S. Pandey, K.K. Pandey, S.M. Mobin, M.C. Puerta, P. Valerga, J. Organomet. Chem. 689 (2004) 1821–1834, https://doi.org/10.1016/j.jorganchem.2004.02.037.
[19] OriginPro9.1., OriginLab Corporation, One Roundhouse Plaza, Suite 303, Northampton, MA 01060, United States, 2014 1800-969-7720. www.OriginLab.com.
[20] Ž.D. Bugarčić, B.V. Petrović, R. Jelić, Transition Met. Chem. 26 (2001) 668–671, https://doi.org/10.1023/A:1012064512961.
[21] A. Hofmann, D. Jaganyi, O.Q. Munro, G. Liehr, R. van Eldik, Inorg. Chem. 42 (2003) 1688–1700, https://doi.org/10.1021/ic020605r.
[22] M. Frisc, G. Trucks, H. Schlegel, G. Scuseria, M. Robb, J. Cheeseman, G. Scalmani, V. Barone, B. Mennucci, G. Petersson, Gaussian 09 (Revision C. 01), Gaussian Inc, Wallingford, (2010).
[23] J. Li, L.-C. Xu, J.-C. Chen, K.-C. Zheng, L.-N. Ji, J. Phys. Chem. A 110 (2006) 8174–8180, https://doi.org/10.1021/jp0564389.
[24] V. Gupta, Principles and Applications of Quantum Chemistry, Elsevier Inc., London, UK, 2015, pp. 156–175.
[25] M. Okamura, M. Yoshida, R. Kuga, K. Sakai, M. Kondo, S. Masaoka, Dalton Trans. 41 (2012) 13081–13089, https://doi.org/10.1039/c2dt30773a.
[26] M. Cossi, G. Scalmani, N. Rega, V. Barone, J. Chem. Phys. 117 (2002) 43–54, https://doi.org/10.1063/1.1480445.
[27] R.G. Parr, L.v. Szentpaly, S. Liu, J. Am. Chem. Soc., 121 (1999) 1922-1924. https://doi.org/10.1021/ja983494x.
[28] R.G. Pearson, Inorg. Chim. Acta. 198 (1992) 781–786, https://doi.org/10.1016/S0020-1693(00)92423-x.
[29] I.M. Wekesa, D. Jaganyi, Dalton Trans. 43 (2014) 2549–2558, https://doi.org/10.1039/c3dt52272e.
[30] R.G. Pearson, J. Mol. Struct. 255 (1992) 261–270, https://doi.org/10.1016/0166-1280(92)85014-c.
[31] F.L. Hirshfeld, Theoret. Chim. Acta. 44 (1977) 129–138, https://doi.org/10.1007/BF00549096.
[32] E.R. Davidson, S. Chakravorty, Theoret. Chim. Acta. 44 (1977) 129–138, https://doi.org/10.1007/BF00549096.
[33] H. Ertürk, R. Puchta, R. van Eldik, Euro. J. Inorg. Chem. 2009 (2009) 1331–1338, https://doi.org/10.1002/ejic.200801135.
[34] A. Hofmann, R. van Eldik, Dalton Trans. (2003) 2979–2985, https://doi.org/10.1039/b305174a.
[35] G. Kinunda, D. Jaganyi, Transition Met. Chem. 39 (2014) 939–949, https://doi.org/10.1007/s11243-014-9879-9.
[36] P.O. Ongoma, D. Jaganyi, Dalton Trans. 42 (2013) 2724–2734, https://doi.org/10.1039/c2dt31956j.
[37] S. Hochreuther, R. Puchta, R. van Eldik, Inorg. Chem. 50 (2011) 8984–8996, https://doi.org/10.1021/ic201151h.
[38] M.S. Davies, J.W. Cox, S.J. Berners-Price, W. Barklage, Y. Qu, N. Farrell, Inorg. Chem. 39 (2000) 1710–1715, https://doi.org/10.1021/ic991104h.
[39] D. Banerjea, in: A Sigel and H Sigel (Eds.), Probing of nucleic acids by metal ion complexes of small molecules, Indian J. Chem A, 36 (1997) 820-820. ISBN 9780824796884.
[40] J.G. Vos, J.M. Kelly, Dalton Trans. (2006) 4869–4883, https://doi.org/10.1039/b606490f.
[41] A. Streitwieser, C.H. Heathcock, E.M. Kosower, P.J. Corfield, Introduction to Organic Chemistry, Macmillan New York, New York, 1992, pp. 971–972.
[42] C.A. Mebi, J. Chem. Sci. 123 (2011) 727–731, https://doi.org/10.1007/s12039-011-0131-2.
[43] J.D. Atwood, Inorganic and Organometallic Reaction Mechanisms, 2nd edition ed., VCH Publishers,1997. pp. 1-18, 47-90.
[44] B. Therrien, Coord. Chem. Rev. 253 (2009) 493–519, https://doi.org/10.1016/j.ccr.2008.04.014.
[45] S. Radisavljević, A.Đ. Kesić, S. Jovanović, B. Petrović, Transition Met. Chem. 43 (2018) 331–338, https://doi.org/10.1007/s11243-018-0221-9.
[46] A. Mambanda, D. Jaganyi, in; R. van Eldik, C. D. Hubbard (Eds.), Inorganic Reaction Mechanisms, Elsevier, 2017, pp. 243-276. https://doi.org/10.1016/bs.adioch.2017.03.001.
[47] J.D. Knoll, B.A. Albani, C.B. Durr, C. Turro, J. Phys. Chem. A 118 (2014) 10603–10610, https://doi.org/10.1021/jp5057732.
[48] S. Chakraborty, P. Munshi, G.K. Lahiri, Polyhedron 18 (1999) 1437–1444, https://doi.org/10.1016/S0277-5387(99)00003-0.
[49] P. Hormnirun, E.L. Marshall, V.C. Gibson, R.I. Pugh, A.J. White, Proc. Natl. Acad. Sci. U.S.A. 103 (2006) 15343–15348, https://doi.org/10.1073/pnas.0602765103.
[50] F. Cherioux, J. Coraux, V. Muller, L. Magaud, N. Bendiab, M. Den Hertog, O. Leynaud, W. Hourani, S. Lamare, D. Kamaruddin, Chem. Eur. J. 23 (2017) 10969–10973, https://doi.org/10.1002/chem.201700054.
[51] U. Fekl, R. van Eldik, C. Richardson, W.T. Robinson, Inorg. Chem. 40 (2001) 3247–3251, https://doi.org/10.1021/ic0009977.
[52] L. Dadci, H. Elias, U. Frey, A. Hoernig, U. Koelle, A.E. Merbach, H. Paulus, J.S. Schneider, Inorg. Chem. 34 (1995) 306–315, https://doi.org/10.1021/ic00105a048.
[53] K. Purkait, S. Chatterjee, S. Karmakar, A. Mukherjee, Dalton Trans. 45 (2016) 8541–8555, https://doi.org/10.1039/c5dt04781a.
[54] Ž.D. Bugarčić, J. Bogojeski, B. Petrović, S. Hochreuther, R. van Eldik, Dalton Trans. 41 (2012) 12329–12345, https://doi.org/10.1039/c2dt31045g.
[55] G.K. Rauth, D. Das, C. Sinha, K. Bag, A. Mahapatra, Transition Met. Chem. 27 (2002) 639–645, https://doi.org/10.1023/A:1019888800542.
[56] T. Das, B. Bera, A. Datta, A. Ghosh, Transition Met. Chem. 34 (2009) 247–253, https://doi.org/10.1007/s11243-009-9185-0.
[57] A. Rilak, B. Petrović, S. Grgurić-Šipka, Ž. Tešić, Ž.D. Bugarčić, Polyhedron 30 (2011) 2339–2344, https://doi.org/10.1016/j.poly.2011.06.019.